

Toward an experimentally determined $^{26}\text{Al}^m(p,\gamma)^{27}\text{Si}$ reaction rate in ONe novae

C. M. Deibel,^{1,2,3,*} J. A. Clark,^{1,†} R. Lewis,^{1,‡} A. Parikh,^{1,§} P. D. Parker,¹ and C. Wrede^{1,||}

¹Wright Nuclear Structure Laboratory, Yale University, New Haven, Connecticut 06520, USA

²Physics Division, Argonne National Laboratory, Argonne, Illinois 60439, USA

³Joint Institute for Nuclear Astrophysics, Michigan State University, East Lansing, Michigan 48824, USA

(Received 25 March 2009; published 29 September 2009)

Strong evidence of the nucleosynthesis of Galactic ^{26}Al has been found through measurements involving excesses in ^{26}Mg from the decay of ^{26}Al in meteoritic inclusions and the 1.809-MeV γ -ray line detected by satellites such as CGRO and INTEGRAL. Several sites for the production of ^{26}Al have been suggested, including ONe novae. Destruction of ^{26}Al in ONe novae is possible via the reactions $^{26}\text{Al}^g(p,\gamma)^{27}\text{Si}$ and $^{26}\text{Al}^m(p,\gamma)^{27}\text{Si}$. In the present work, resonance parameters for the $^{26}\text{Al}^m(p,\gamma)^{27}\text{Si}$ reaction have been determined via studies of the $^{27}\text{Al}(^3\text{He},t)^{27}\text{Si}^*(p)^{26}\text{Al}^m$ and $^{28}\text{Si}(^3\text{He},\alpha)^{27}\text{Si}^*(p)^{26}\text{Al}^m$ reactions. Several new $^{26}\text{Al}^m + p$ resonances have been discovered within 1 MeV above the proton threshold of 7.691 MeV. Excitation energies and proton-branching ratios for those and previously known states are reported.

DOI: [10.1103/PhysRevC.80.035806](https://doi.org/10.1103/PhysRevC.80.035806)

PACS number(s): 25.40.Lw, 26.30.Ca, 27.30.+t, 97.30.Qt

I. INTRODUCTION

The 7.2×10^5 yr half-life of the ^{26}Al ground state (hereafter $^{26}\text{Al}^g$), which is short on the time scales of Galactic chemical evolution ($\sim\text{Gyr}$), makes this nucleus a favorable candidate for studying ongoing nucleosynthesis in the Galaxy. The observation of ^{26}Mg excesses that are linearly proportional to ^{27}Al content in minerals extracted from the Allende meteorite [1,2] suggested the inclusion and subsequent *in situ* decay of ^{26}Al in these minerals, giving the first evidence of the presence of ^{26}Al in our Galaxy at the time of formation of our Solar System. Since that initial discovery, several presolar grains with isotopic abundances that suggest nova origins have been found, including two that have had their $^{26}\text{Al}/^{27}\text{Al}$ ratios measured to be quite high ($>10^{-2}$) relative to solar abundances [3], although the nova origin of these grains has been called into question [4].

About 99.7% of the time, $^{26}\text{Al}^g$ β^+ decays through the first excited state of ^{26}Mg , which promptly emits a 1.809-MeV γ ray as it decays to its ground state. This 1.809-MeV γ -ray line produced in the Galaxy was first detected by the HEAO-3 satellite experiment [5]. Since then, its existence has been confirmed by several balloon-borne [6,7] and satellite missions [8,9], and, most recently, by the INTEGRAL satellite, which detected approximately $2.8M_\odot$ of Galactic steady-state ^{26}Al [10]. Several sites have been suggested to contain environments where ^{26}Al may be produced, including supernovae, asymptotic giant branch (AGB) stars, Wolf Rayet stars, and

oxygen neon (ONe) novae. While recent studies suggest the majority of ^{26}Al is synthesized in more massive stellar events [10], such as core-collapse supernovae, an important contribution from ONe novae cannot be ruled out [11,12].

The production of ^{26}Al is complicated by the existence of an isomeric state ($^{26}\text{Al}^m$) located at 228 keV, with $J^\pi = 0^+$ and $t_{1/2} = 6.3$ s. While the direct M5 electromagnetic transition of the isomer to the $J^\pi = 5^+$ ground state is slow ($\sim 8 \times 10^5$ yr [13]) compared with the isomer's lifetime, it was previously shown in Ref. [14] that $^{26}\text{Al}^g$ and $^{26}\text{Al}^m$ come into thermal equilibrium at temperatures greater than 0.4 GK; however, for stellar environments below this temperature, such as ONe novae, the authors of Ref. [14] make the case that the two levels must be treated separately. This issue has been reexamined more recently and is somewhat more subtle, and it is not clear when or if $^{26}\text{Al}^g$ and $^{26}\text{Al}^m$ will reach thermal equilibrium [15]. Rather, the authors of Ref. [15] have shown that $^{26}\text{Al}^g$ and $^{26}\text{Al}^m$ do communicate through higher lying levels at temperatures below 0.4 GK, and while the two should be entered separately in reaction rate networks, the effective decay rate, which depends on this communication, must be used. Furthermore, the relationship between $^{26}\text{Al}^g$ and $^{26}\text{Al}^m$ depends on not only the temperature, but also the time scales of nuclear reactions and equilibration. Therefore, reactions involving the isomeric state of ^{26}Al may also be important at temperatures higher than 0.4 GK, which exist in more massive stellar events, which may produce the majority of Galactic ^{26}Al . The situation as it pertains to nova nucleosynthesis, where $T \leq 0.4$ GK, is discussed below.

In ONe novae, ^{26}Al is produced in the MgAl cycle via the reaction sequence $^{24}\text{Mg}(p,\gamma)^{25}\text{Al}(\beta^+\nu_e)^{25}\text{Mg}(p,\gamma)^{26}\text{Al}$, where proton capture on ^{25}Mg can lead to either the ground state or the isomeric state of ^{26}Al (Fig. 1). The former leads to the β^+ -delayed 1.809-MeV γ ray, while the isomeric state decays directly to the ground state of ^{26}Mg , bypassing the emission of the 1.809-MeV γ ray. Additionally, the nucleosynthesis of ^{26}Al is further complicated at ONe novae temperatures ($T_{\text{peak}} = 0.1\text{--}0.4$ GK) where the $^{25}\text{Al}(p,\gamma)$ reaction competes with the β^+ decay of ^{25}Al , and $^{26}\text{Al}^m$ is produced via

* deibel@phy.anl.gov

[†]Present address: Physics Division, Argonne National Laboratory, Argonne, Illinois 60439, USA.

[‡]Present address: Sauder School of Business, University of British Columbia, Vancouver, British Columbia V6T 1Z2, Canada.

[§]Present address: Physik Department E12, Technische Universität München, D-85748 Garching, Germany.

^{||}Present address: Department of Physics, University of Washington, Seattle, Washington 98195, USA.

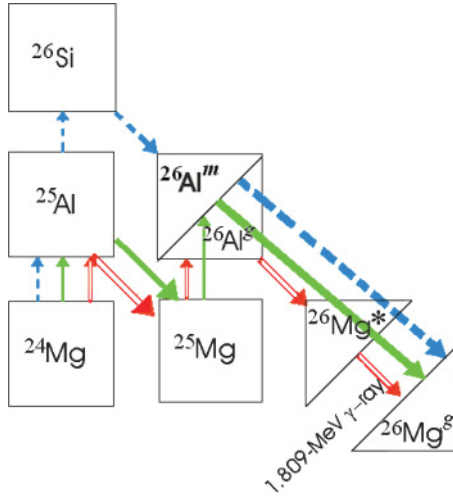


FIG. 1. (Color online) Three reaction sequences that produce $^{26}\text{Al}^g$ and $^{26}\text{Al}^m$ at nova temperatures (0.1–0.4 GK).

the $^{24}\text{Mg}(p,\gamma)^{25}\text{Al}(p,\gamma)^{26}\text{Si}(\beta^+\nu_e)^{26}\text{Al}^m$ reaction sequence (Fig. 1), where the β^+ decay of $^{26}\text{Al}^m$ will then bypass the 1.809-MeV γ -ray emission. In each of these scenarios, the main destruction mechanism of ^{26}Al in novae is proton capture on either $^{26}\text{Al}^g$ or $^{26}\text{Al}^m$. Previous experimental studies of the destruction of ^{26}Al have focused solely on the $^{26}\text{Al}^g(p,\gamma)$ reaction [12,16–18]; although proton capture on the isomer could affect overall ^{26}Al production, there is very little direct experimental information known about $^{26}\text{Al}^m(p,\gamma)$ [19] and no published information on any $^{26}\text{Al}^m + p$ resonances.

For isolated, narrow resonances, the resonant component of the reaction rate in $\text{cm}^3 \text{mol}^{-1} \text{s}^{-1}$ is given by

$$N_A \langle \sigma v \rangle = 1.54 \times 10^{11} (\mu T_9)^{-3/2} \times \sum_r (\omega\gamma)_r \exp(-11.605 E_r / T_9), \quad (1)$$

where T_9 is the temperature in GK, E_r is the energy of the ^{27}Si resonance in MeV, μ is the reduced mass in u, and $(\omega\gamma)_r$ is the resonance strength in MeV, given by

$$(\omega\gamma)_r = \frac{(2J_r + 1)}{(2J_{26\text{Al}} + 1)(2J_p + 1)} \frac{\Gamma_p \Gamma_\gamma}{\Gamma}. \quad (2)$$

The exponential dependence on the energies of the resonances can be seen in Eq. (1). Additionally, the resonance strengths [Eq. (2)] depend on the partial proton and γ widths, Γ_p and Γ_γ , respectively, the total width, $\Gamma_p + \Gamma_\gamma = \Gamma$, and the spins of the resonances (J_r) and reactants (J_p and $J_{26\text{Al}}$). Previous calculations of the $^{26}\text{Al}^m(p,\gamma)^{27}\text{Si}$ rate $\langle \sigma v \rangle_m$ were based on experimental information from the $^{26}\text{Al}^g(p,\gamma)^{27}\text{Si}$ reaction and Hauser-Feshbach (HF) calculations and were determined [20] using

$$\langle \sigma v \rangle_m = \langle \sigma v \rangle_g \frac{[\langle \sigma v \rangle_m]_{\text{HF}}}{[\langle \sigma v \rangle_g]_{\text{HF}}}. \quad (3)$$

Clearly, if the structures of the $^{26}\text{Al}^g + p$ resonances and the $^{26}\text{Al}^m + p$ resonances are different, a rate based on the scaling shown in Eq. (3) may not be meaningful, and one based on

actual experimental information is necessary. In the sections below, we present the first experimentally determined information on $^{26}\text{Al}^m(p,\gamma)^{27}\text{Si}$ resonances, including previously unpublished levels in ^{27}Si and proton-branching ratios.

II. EXPERIMENT

The two transfer reactions $^{27}\text{Al}(^3\text{He},t)^{27}\text{Si}^*$ and $^{28}\text{Si}(^3\text{He},\alpha)^{27}\text{Si}^*$ were studied [21] at the Wright Nuclear Structure Laboratory at Yale University using the extended stretched transuranium (ESTU) tandem Van de Graaff accelerator. The structure of ^{27}Si above the proton threshold has been studied previously using both of these reactions [17,22] and through direct measurements of the $^{26}\text{Al}^g(p,\gamma)$ [12,16] reaction and $^{27}\text{P}(\beta^+\nu_e)$ [23]. Here we present results of coincidence measurements, studying the proton decay of $^{26}\text{Al}^m + p$ resonances. $^3\text{He}^{2+}$ beams of 25 MeV (at a current of 30 pA) and of 17.5 MeV (with a typical current of 5 pA) were used for the $^{27}\text{Al}(^3\text{He},t)^{27}\text{Si}^*$ and $^{28}\text{Si}(^3\text{He},\alpha)^{27}\text{Si}^*$ reactions, respectively. A $58\text{-}\mu\text{g}/\text{cm}^2$ ^{27}Al target on a $20\text{-}\mu\text{g}/\text{cm}^2$ carbon substrate and a $311\text{-}\mu\text{g}/\text{cm}^2$ self-supporting Si target were used, and their thicknesses were measured with a 10% uncertainty via energy loss of 5.486-MeV α particles from a ^{241}Am source. The reaction products were momentum analyzed using an Enge split-pole spectrograph and detected by a position-sensitive ionization drift chamber (PIDC) filled with 150 torr of isobutane gas, which was placed at the focal plane and backed by a plastic scintillator [24]. The PIDC is used to measure position along the focal plane via front and rear wires with delay chip readouts, and energy loss in the drift region, ΔE , via a cathode, while the scintillator is used to determine the residual energy of the particles, E_{res} . For the $^{27}\text{Al}(^3\text{He},t)^{27}\text{Si}^*$ reaction, the entrance aperture of the spectrograph was set at ± 20 and ± 40 mrad in the horizontal and vertical directions, respectively, and a field strength of 10.8 kG was used. The $^{28}\text{Si}(^3\text{He},\alpha)^{27}\text{Si}^*$ reaction was studied with the aperture at ± 10 mrad in the horizontal direction and ± 40 mrad in the vertical direction and with a field strength of 6.1 kG.

Protons emitted from excited states in ^{27}Si were detected by the Yale lamp-shade array (YLSA), an array of five 16-strip silicon detectors¹ arranged in a lamp-shade configuration [21]. YLSA was positioned to cover backward angles, and the detectors, which were tilted forward, covered an angular range of $\theta_{\text{lab}} = 131^\circ$ to $\theta_{\text{lab}} = 166^\circ$. The spectrograph was placed at a 3° angle with respect to the beam axis to avoid prohibitively large event rates due to the forward scattered beam at 0° to 2° . Monte Carlo simulations showed there was not a significant difference in the proton hit patterns in YLSA between measurements taken at 3° compared with 0° . Additionally, at such a small angle, magnetic substates with $m \neq 0$ will have negligible contributions.

¹Micron Semiconductor Ltd. Model YY1.

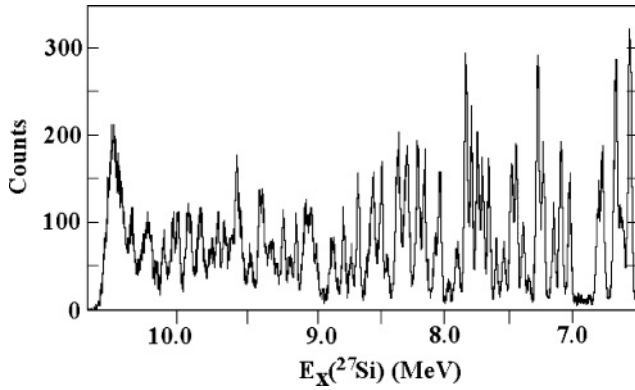


FIG. 2. Focal-plane spectrum of the tritons (labeled with corresponding excitation energy in ^{27}Si) from the $^{27}\text{Al}(^3\text{He},t)^{27}\text{Si}$ reaction.

III. DATA

A. $^{27}\text{Al}(^3\text{He},t)^{27}\text{Si}^*$

The reaction products were separated from one another and identified by plotting the cathode (ΔE), scintillator (E_{res}), and the focal-plane position signals in two-dimensional histograms. Once identified, the tritons were then cleanly selected to obtain a spectrum of the excited states in ^{27}Si populated via the $^{27}\text{Al}(^3\text{He},t)^{27}\text{Si}^*$ charge-exchange reaction (Fig. 2). The triton spectrum has approximately 35-keV full width at half maximum (FWHM) resolution, and the peaks therein were fit with a Gaussian function when isolated, or a multi-Gaussian function when several peaks overlapped. Excitation energies for states in ^{27}Si were determined by using well-known states from several reactions to calibrate the focal plane. A polynomial of the radius of curvature in the spectrograph, ρ , as a function of the channel number was fit to the known peaks along the focal plane. For the initial focal-plane calibration, known peaks [25] from the $^{13}\text{C}(^3\text{He},\alpha)^{12}\text{C}$ reaction were used to determine the approximate excitation energies of states in ^{27}Si . Once those were determined, known isolated states in ^{27}Si [$E_x = 7.005(8)$, $7.383(4)$, $7.972(2)$, and $8.671(3)$ MeV [25]] were used to perform an internal calibration for states below $E_x = 8.671$ MeV. For states above this region, ^{32}Cl states at $E_x = 0.0$, $0.0899(1)$, $0.4661(1)$, $1.1685(2)$, $1.719(4)$, and $2.122(5)$ MeV [25] populated by the $^{32}\text{S}(^3\text{He},t)^{32}\text{Cl}$ reaction were used in conjunction with the ^{27}Si states as a calibration. Energies for ^{27}Si states below $E_x = 8.671$ MeV were calculated two ways: by using either the two calibrations described above or the internal calibration only. For both calibrations, a second-degree polynomial fit was used, and the two sets of energies determined using the different calibrations were found to be the same to within the calculated uncertainty. The excitation energies found using the ^{32}Cl and internal calibration ($\chi^2/\nu = 0.66$) were taken as the final excitation energies determined with the $^{27}\text{Al}(^3\text{He},t)^{27}\text{Si}^*$ reaction.

B. $^{28}\text{Si}(^3\text{He},\alpha)^{27}\text{Si}^*$

For the $^{28}\text{Si}(^3\text{He},\alpha)^{27}\text{Si}^*$ transfer reaction, the α particles were selected and a spectrum (Fig. 3) of the excited

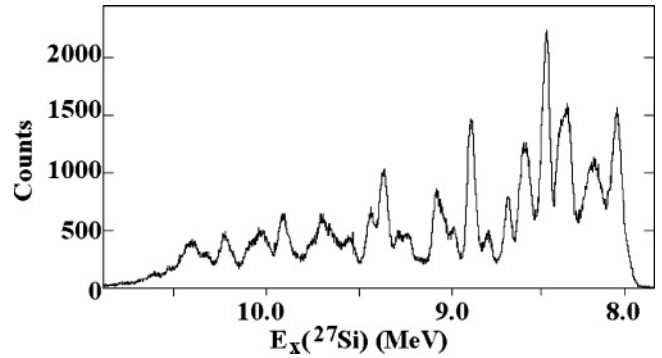


FIG. 3. Focal-plane spectrum of the α particles (labeled with corresponding excitation energy in ^{27}Si) from the $^{28}\text{Si}(^3\text{He},\alpha)^{27}\text{Si}$ reaction.

states in ^{27}Si was obtained in the same way as described previously.

Due to the reaction kinematics, the dispersion at the focal plane was worse for this reaction than for the $^{27}\text{Al}(^3\text{He},t)$ reaction, and a resolution of approximately 80 keV was obtained. As a result, many individual peaks in the singles spectrum could not be resolved. However, the analysis of the coincidence spectra (described below) allowed the ^{27}Si peaks to be further separated based on their decay modes and subsequently fit in the same manner as the $^{27}\text{Al}(^3\text{He},t)^{27}\text{Si}$ spectrum. To calibrate the focal plane, the $^{12}\text{C}(^3\text{He},\alpha)^{11}\text{C}$ transfer reaction was measured, and well-known ^{11}C excitation energies [$E_x = 6.3392(14)$, $6.4782(13)$, $6.9048(14)$, $7.4997(15)$, $8.1045(17)$, $8.420(2)$, $8.655(8)$, and $8.699(10)$ MeV [25]] were used, resulting in a second-order fit with $\chi^2/\nu = 1.05$. A weighted average of the ^{27}Si excitation energies determined from the $^{28}\text{Si}(^3\text{He},\alpha)^{27}\text{Si}$ reaction and those determined via the $^{27}\text{Al}(^3\text{He},t)^{27}\text{Si}$ reaction was taken to determine the excitation energies of ^{27}Si states (Table I).

C. Coincidence data

Protons emitted from states in ^{27}Si above the proton thresholds ($S_p = 7.463$ MeV, $S_p = 7.691$ MeV, and $S_p = 7.880$ MeV for decays to the ground, isomeric, and second excited states, respectively) populated via the $^{27}\text{Al}(^3\text{He},t)^{27}\text{Si}$ and $^{28}\text{Si}(^3\text{He},\alpha)^{27}\text{Si}$ reactions were detected by YLSA. The dependence of the proton energies on the energies of the excited ^{27}Si levels can be seen in the resulting two-dimensional spectra of proton energy vs focal-plane position of the residual products (Figs. 4 and 5).

The three strongest diagonal lines seen in Figs. 4 and 5, which correspond to proton decays to the ground, isomeric, and second excited states, are well separated so that proton decays to specific ^{26}Al states can be selected to produce focal-plane spectra corresponding to each particular decay channel, which are then projected onto the momentum axis (Figs. 6 and 7). The resulting focal-plane spectra of the α particles detected in coincidence with proton decays to the ground, isomeric, and second excited states from the $^{28}\text{Si}(^3\text{He},\alpha)^{27}\text{Si}^*(p)^{26}\text{Al}$ reaction allow specific states in ^{27}Si to be identified, despite the poor dispersion in the original focal-plane spectrum of all the detected α particles (Fig. 8). These peaks from the

TABLE I. Excitation energies (in MeV) of ^{27}Si levels found in the literature [25] and via the two transfer reactions described in this work. The weighted average of the ^{27}Si levels determined from the two transfer reactions studied here is also shown.

| Previous work [25] | Present work | | Weighted average |
|--------------------|---|--|------------------|
| | $^{27}\text{Al}(^3\text{He},t)^{27}\text{Si}$ | $^{28}\text{Si}(^3\text{He},\alpha)^{27}\text{Si}$ | |
| 8.140(4) | | 8.136(4) | 8.136(4) |
| 8.157(2) | | 8.156(5) | 8.156(5) |
| 8.165(2) | 8.162(2) | | 8.162(2) |
| 8.176(2) | | | |
| 8.184(4) | | | |
| 8.207(3) | 8.211(5) | 8.208(9) | 8.210(4) |
| 8.226(3) | | | |
| 8.289(3) | 8.299(5) | | 8.299(5) |
| 8.328(2) | 8.324(5) | 8.312(4) | 8.318(3) |
| 8.358(2) | 8.358(4) | 8.350(4) | 8.354(3) |
| | 8.380(4) | 8.369(4) | 8.375(3) |
| 8.451(2) | 8.450(4) | 8.440(5) | 8.446(3) |
| | 8.493(4) | 8.476(5) | 8.486(3) |
| | 8.525(4) | 8.521(5) | 8.523(3) |
| 8.545(3) | 8.558(4) | 8.556(5) | 8.557(3) |
| | 8587(4) | 8.582(5) | 8.586(3) |
| 8.671(3) | 8.671(3) ^a | 8.660(5) | 8.668(3) |
| | 8.724(4) | | 8.724(4) |
| 8.777(5) | | 8.777(5) | 8.777(5) |
| | 8.782(4) | | 8.782(4) |
| | | 8.822(5) | 8.822(5) |
| | 8.863(3) | 8.867(5) | 8.864(3) |
| | | 8.872(5) | 8.872(5) |
| | 8.947(9) | 8.926(5) | 8.931(4) |
| | 8.987(3) | 8.974(5) | 8.984(3) |
| | 9.028(3) | 9.021(5) | 9.026(3) |
| 9.067(4) | | 9.066(5) | 9.066(5) |
| | 9.072(3) | 9.081(5) | 9.074(3) |
| | 9.140(2) | 9.138(12) | 9.140(2) |
| | | 9.164(12) | 9.164(12) |
| | 9.184(3) | | 9.184(3) |
| | | 9.215(4) | 9.215(4) |
| | 9.227(4) | | 9.227(4) |
| | 9.238(4) | 9.236(2) | 9.237(2) |
| | | 9.256(4) | 9.256(4) |
| | 9.280(5) | 9.273(2) | 9.274(2) |
| | 9.311(3) | 9.291(8) | 9.308(3) |
| | 9.335(7) | 9.345(9) | 9.339(6) |
| | 9.362(10) | 9.363(4) | 9.363(4) |
| | 9.386(13) | | 9.386(13) |
| | 9.409(3) | | 9.409(3) |
| | | 9.428(3) | 9.428(3) |
| | | 9.438(18) | 9.438(18) |
| | 9.477(3) | | 9.477(3) |
| | 9.549(10) | 9.547(4) | 9.547(4) |
| | 9.577(3) | 9.575(2) | 9.576(4) |
| | 9.616(9) | 9.615(7) | 9.615(6) |
| | 9.666(10) | 9.652(5) | 9.655(4) |
| | 9.715(2) | 9.714(3) | 9.715(2) |
| | 9.762(2) | 9.767(2) | 9.764(2) |
| | | 9.791(2) | 9.791(2) |
| | 9.834(2) | | 9.834(2) |
| | 9.856(3) | | 9.856(3) |

TABLE I. (Continued.)

| Previous work [25] | Present work | | Weighted average |
|--------------------|---|--|------------------|
| | $^{27}\text{Al}(^3\text{He},t)^{27}\text{Si}$ | $^{28}\text{Si}(^3\text{He},\alpha)^{27}\text{Si}$ | |
| | | 9.895(2) | 9.895(2) |
| | 9.914(2) | 9.918(2) | 9.916(2) |
| | 9.934(5) | | 9.934(5) |

^aUsed in energy calibration.

coincidence spectra were used to determine the energies of ^{27}Si levels populated by the $^{28}\text{Si}(^3\text{He},\alpha)^{27}\text{Si}$ reaction and are found in Table I.

IV. ANGULAR CORRELATIONS

The angular distribution of the proton decays from excited states in ^{27}Si , with respect to the residual reaction particles, depends on the spins of the products involved. This angular correlation can be described via a sum of Legendre polynomials [26,27]:

$$W(\theta) = \sum_{k=0,2,\dots} A_k P_k(\cos\theta), \quad (4)$$

where the sum over k determines the angular momentum transfer, as $k = 2l$. Since the spins of the resonances are not known, the coefficients A_k are left as free parameters when Eq. (4) is fit to the angular distribution of the proton decays. In principle, the angular correlation data could consist of 16 points, corresponding to the 16 strips in YLSA. However, to increase the number of counts in each angular bin, the data were sorted into four-strip bins with typical $\theta_{\text{c.m.}}$ centered at 163.2° , 155.0° , 145.6° , and 135.9° , with typical ranges of 5.6° , 6.5° , 7.6° , and 8.3° , respectively, which are determined by Monte Carlo simulations based on the geometry of YLSA and the kinematics of the system. For each four-strip bin, the areas of the peaks of interest are found using Gaussian fits

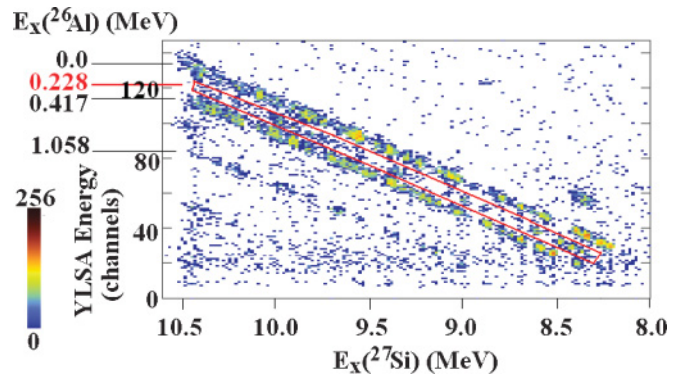


FIG. 4. (Color online) Spectrum of proton energy detected by YLSA vs focal-plane position of coincident tritons (labeled with corresponding excitation energy in ^{27}Si) from the $^{27}\text{Al}(^3\text{He},t)^{27}\text{Si}^*(p)^{26}\text{Al}$ reaction. The energies of states in ^{26}Al to which the protons decay are labeled to the left of the y axis and correspond to the diagonal bands shown. A gate (red) around the 228-keV band is shown to guide the reader. Color represents intensity.

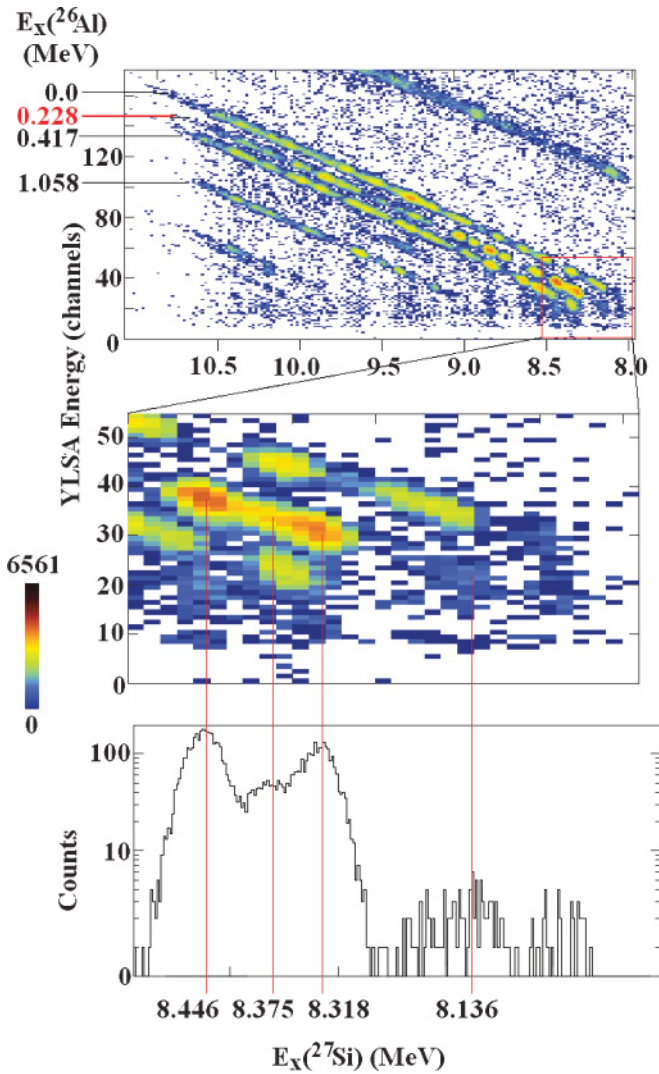


FIG. 5. (Color online) Spectrum of decay-proton energy detected by YLSA vs focal-plane position of coincident α particles (labeled with corresponding excitation energy in ^{27}Si) from the $^{28}\text{Si}(^3\text{He},\alpha)^{27}\text{Si}^*(p)^{26}\text{Al}$ reaction (top panel), with the low-energy portion of the spectrum enlarged (middle panel) to show ^{27}Si states with the lowest energies, which decayed to $^{26}\text{Al}^m$ (bottom panel). The energies of states in ^{26}Al to which the protons decay are labeled to the left of the y axis on the top panel and correspond to the diagonal bands shown. Color represents intensity.

with the peak centroids and widths fixed to the same values as used previously when determining excitation energies. Unfortunately, the statistics for the coincidence spectra from the $^{27}\text{Al}(^3\text{He},t)^{27}\text{Si}^*(p)^{26}\text{Al}$ reaction were too low even when four-strip bins were used. Therefore, angular correlations, and the subsequent Γ_p/Γ determinations, could only be measured for the $^{28}\text{Si}(^3\text{He},\alpha)^{27}\text{Si}^*(p)^{26}\text{Al}$ data. Once the areas of the peaks were determined, they were corrected for the geometrical efficiency of the four-strip bins and for the accidental coincidences from the background in YLSA. The ratio of the corrected area of the coincidence data to the area of the original focal-plane data was taken for each peak. This value was then plotted as a function of $\theta_{c.m.}$ for each bin and fit

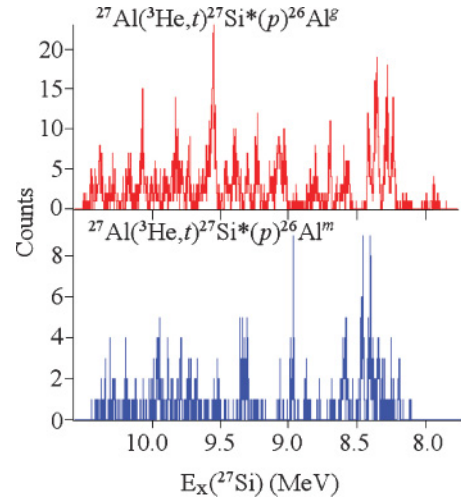


FIG. 6. (Color online) Focal-plane position spectra of tritons (labeled with corresponding excitation energy in ^{27}Si) detected in coincidence with protons decaying to the ground state of ^{26}Al from the $^{27}\text{Al}(^3\text{He},t)^{27}\text{Si}^*(p)^{26}\text{Al}^g$ reaction (top panel) and in coincidence with protons decaying to the isomeric state of ^{26}Al from the $^{27}\text{Al}(^3\text{He},t)^{27}\text{Si}^*(p)^{26}\text{Al}^m$ reaction (bottom panel). Note the difference in the vertical scales.

using Eq. (4). The fits were constrained so that the unphysical scenarios of $\Gamma_p/\Gamma < 0$ and $\Gamma_p/\Gamma > 1$ were not solutions. The fitting was done using a χ^2_p p -value analysis, where terms were added to the sum in Eq. (4) until a fit was achieved that had a p value of >0.05 [28], which corresponded to a lower limit for the l transfer of each decay, l_{\min} (Fig. 9). This l_{\min} can provide tentative constraints on the J^π values for the resonances. By integrating Eq. (4) over the entire range $\theta_{c.m.} = [0,\pi]$, the branching ratio Γ_p/Γ of each decay was determined. These branching ratios were then normalized on the basis of similar

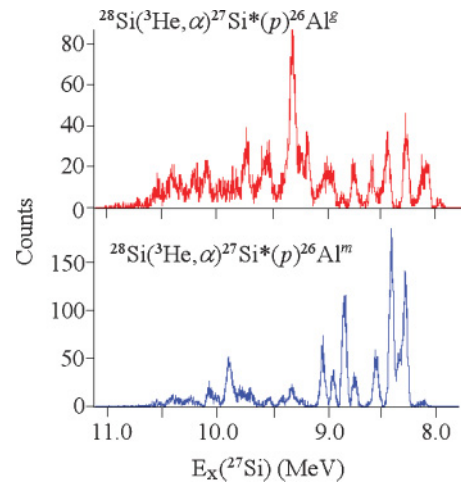


FIG. 7. (Color online) Focal-plane position spectra of α particles (labeled with corresponding excitation energy in ^{27}Si) detected in coincidence with protons decaying to the ground state of ^{26}Al from the $^{28}\text{Si}(^3\text{He},\alpha)^{27}\text{Si}^*(p)^{26}\text{Al}^g$ reaction (top panel) and in coincidence with protons decaying to the isomeric state of ^{26}Al from the $^{28}\text{Si}(^3\text{He},\alpha)^{27}\text{Si}^*(p)^{26}\text{Al}^m$ reaction (bottom panel). Note the difference in the vertical scales.

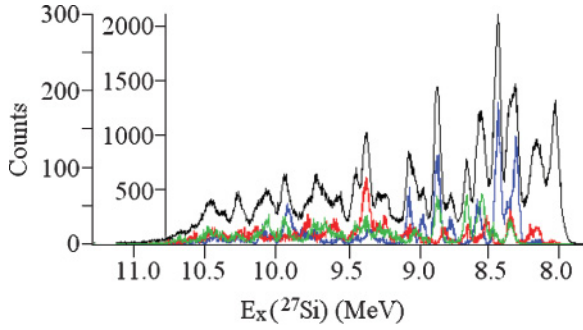


FIG. 8. (Color online) Focal-plane position spectra of coincident α particles (labeled with corresponding excitation energy in ^{27}Si) from the $^{28}\text{Si}(^3\text{He}, \alpha)^{27}\text{Si}^*(p)^{26}\text{Al}^8$ (red), $^{28}\text{Si}(^3\text{He}, \alpha)^{27}\text{Si}^*(p)^{26}\text{Al}^m$ (blue), and $^{28}\text{Si}(^3\text{He}, \alpha)^{27}\text{Si}^*(p)^{26}\text{Al}^*$ (green) reactions, overlaid with the original focal-plane position spectrum for all detected α particles (black). To aid the reader, the left-most y axis refers to the coincident data and has been scaled to a comparable amplitude to the original α -particle spectrum (right-most y axis).

branching-ratio measurements from $^{12}\text{C}(^3\text{He}, p)^{14}\text{N}^*(p)^{13}\text{C}$ coincidence data involving well-known ^{14}N states at $E_x = 8.618(2)$, $9.388(3)$, and $9.703(4)$ MeV with proton-branching ratios of 99.86%, 100%, and 99.99959%, respectively [25], which differed from our measured values by 34(19)%. These data were collected during the same experimental run as the $^{28}\text{Si}(^3\text{He}, \alpha)^{27}\text{Si}^*(p)^{26}\text{Al}$ measurement in order to correct for any systematic errors, such as dead-time corrections. The main source of error in the branching ratios comes from the background determination in the total focal-plane spectrum. As no section of the spectrum was free of peaks, only a range of possible backgrounds could be determined (approximately 0–200 counts/channel), and the error resulting from that range is typically much larger than any systematic or statistical errors in the measurement. As the background is subtracted from the peak areas in the spectrum of all α particles detected at the focal plane, only the overall scale of the angular distribution changes while the shape of the distribution remains the same. Therefore, this background uncertainty does not affect the angular momentum transfer assignments. The final branching ratios are listed in Table II.

V. RESULTS AND CONCLUSIONS

All angular momentum transfers for proton decays to $^{26}\text{Al}^m$, with the exception of the 8.375-MeV state and those states for which l_{\min} could not be determined, were found to be consistent with $l = 0$, which corresponds to a minimum spin of $J = 1/2$. This value was used for all resonances, and thus the spin factor in Eq. (2) is unity. The resonance strengths $\omega\gamma$ for all states were calculated with Γ_p/Γ taken from Table II, and the Γ_γ are taken to be 1 eV, based on the rough average of Γ_γ values found for levels near the proton threshold in nuclides of similar mass [29]. Therefore, the strength of each resonance was the Γ_p/Γ value found in Table II multiplied by 1 eV. These values, along with the resonance energies also found in Table II, were used in Eq. (1) to determine the $^{26}\text{Al}^m(p, \gamma)^{27}\text{Si}$

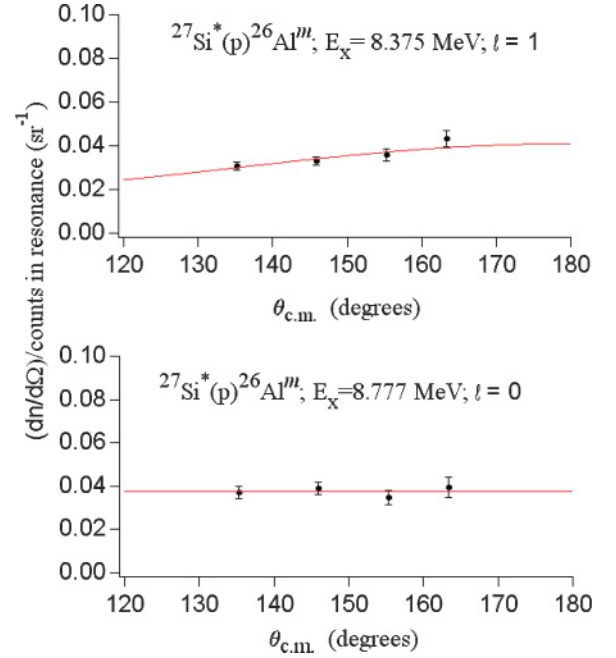


FIG. 9. (Color online) Typical angular correlations for proton decays from excited states in ^{27}Si [populated via the $^{28}\text{Si}(^3\text{He}, \alpha)$ reaction] to $^{26}\text{Al}^m$ fit with Eq. (4). The $dn/d\Omega$ shown here are found using the limit of zero background, and the angle is the centroid of the angular bin expressed in c.m. (see text for more details).

reaction rate for typical ONe novae peak temperatures (0.1–0.4 GK) (Fig. 10).

The $^{26}\text{Al}^m(p, \gamma)^{27}\text{Si}$ rate calculated here is dominated (not surprisingly) by the lowest resonance we could measure, corresponding to $E_r = 445$ keV ($E_x = 8.136$ MeV), which is shown directly under the total reaction rate in Fig. 10. Because of the detection threshold of YLSA, however, coincidence data

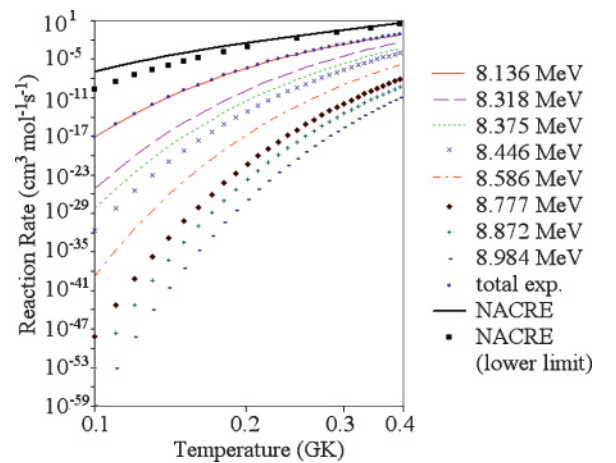


FIG. 10. (Color online) Contributions to the $^{26}\text{Al}^m(p, \gamma)^{27}\text{Si}$ reaction rate from the ^{27}Si resonances studied herein. The total reaction rate (blue dots) (which is likely a lower limit due to the inability to detect protons of energies much less than 445 keV) is plotted directly on top of the contribution from the 8.136-MeV state in ^{27}Si (solid red line). The value found by the NACRE Collaboration using Eq. (3) [20] (solid black line) is shown for comparison.

TABLE II. Resonance energies, minimum l transfers (l_{\min}), and branching ratios for proton decays from excited states in ^{27}Si , populated via the $^{28}\text{Si}(^3\text{He},\alpha)^{27}\text{Si}$ reaction, to the ground, isomeric, and second excited states in ^{26}Al .

| E_x (^{27}Si) (MeV) | Ground state | | | Isomeric state | | | 2nd excited state | | |
|----------------------------------|--------------|--------------|-----------------------|----------------|--------------|-----------------------|-------------------|------------|-----------------------|
| | E_r (keV) | l_{\min} | $\Gamma_p/\Gamma(\%)$ | E_r (keV) | l_{\min} | $\Gamma_p/\Gamma(\%)$ | E_r (keV) | l_{\min} | $\Gamma_p/\Gamma(\%)$ |
| 8.136 | | | | 445 | 0 | $\geq 4(1)$ | | | |
| 8.156 | 693 | 0 | 22(4) | | | | | | |
| 8.210 | 747 | 0 | 15(4) | | | | | | |
| 8.318 | | | | 627 | 0 | 53(10) | | | |
| 8.354 | 891 | 0 | 39(6) | | | | 474 | 0 | 28(4) |
| 8.375 | | | | 684 | 1 | 31(8) | | | |
| 8.446 | | | | 755 | ^a | 47(7) ^b | | | |
| 8.486 | | | | | | | 606 | 0 | 22(5) |
| 8.523 | 1060 | 0 | 39(12) | | | | | | |
| 8.557 | 1094 | ^a | 36(20) | | | | 677 | 0 | 35(17) |
| 8.586 | | | | 895 | 0 | 40(9) | | | |
| 8.668 | 1205 | 0 | 16(5) | | | | 788 | 0 | 48(13) |
| 8.777 | | | | 1086 | 0 | 60(26) | | | |
| 8.822 | 1359 | 0 | 72(39) | | | | | | |
| 8.864 | | | | | | | 984 | 0 | 94(13) |
| 8.872 | | | | 1181 | 0 | 58(11) | | | |
| 8.931 | 1468 | 0 | 100(100) ^c | | | | | | |
| 8.984 | | | | 1293 | 0 | 28(10) | | | |

^a l_{\min} could not be determined for this decay.

^bThe uncertainty in Γ_p/Γ is not dominated by the background uncertainty for this case.

^cThe uncertainty introduced by the unknown spectrum background produced a result that was consistent with both 0 and 100%.

from states with $E_r < 445$ keV, nine of which are above the proton threshold, could not be measured. Indeed, as $E_r = 445$ keV for the 8.136-MeV state, the energies of the decay protons are at the detector's energy threshold. Therefore, it is likely that some of the decay protons from this state are not detected, and its contribution to the reaction rate should be taken as a lower limit. As a result, the total reaction rate found here is most likely a lower limit, since the resonances that may dominate the rate are not included. This may explain some of the discrepancies when compared with the reaction rate calculated by the NACRE Collaboration [20] using Eq. (3), which is higher by 2–10 orders of magnitude at ONe novae temperatures. The use of lower limits for the l transfers, which correspond to $J = 1/2$, is consistent with the interpretation of this reaction rate as a lower limit. Furthermore, any increase in the J^π values of the resonances would not cause an overall increase of ≥ 2 orders of magnitude in the total rate, making any J^π assignment consistent with a rate much less than the NACRE calculation.

Our results show that the results of the NACRE calculation may not be very realistic, because of the stark differences seen in the proton decays to the $^{26}\text{Al}^g$ and $^{26}\text{Al}^m$ states from levels in ^{27}Si . As shown in Figs. 6–8, proton decays to $^{26}\text{Al}^g$ and $^{26}\text{Al}^m$ most often come, not surprisingly, from different states in ^{27}Si with different probabilities. Thus, any $^{26}\text{Al}^m + p$ calculation based on $^{26}\text{Al}^g + p$ resonance strengths may be unrealistic, and a reaction rate calculation based on experimentally determined information for the $^{26}\text{Al}^m(p,\gamma)^{27}\text{Si}$ reaction is currently needed to give more meaningful information on its role in the production of Galactic ^{26}Al .

The overall effect of the $^{26}\text{Al}^m(p,\gamma)^{27}\text{Si}$ reaction rate on ^{26}Al produced in ONe novae is outside the scope of this work, as the reaction rate for typical ONe novae temperatures is most likely dominated by resonances lower in energy than those reported here because of the location of the Gamow peak centered at 330 keV. The consequences of the levels determined in this work for astrophysical environments with higher temperatures (~ 0.6 to 7 GK, where these levels are located in the Gamow window) will be discussed elsewhere [30]. Additionally, other reaction rates exist whose uncertainties influence ^{26}Al production. Principally, uncertainties in the $^{25}\text{Al}(p,\gamma)^{26}\text{Si}$ reaction rate previously resulted in approximately a factor of 3 uncertainty in the amount of ^{26}Al ejected in ONe novae according to current models [31]. While recent work has reduced this uncertainty [32,33], a direct measurement of the resonance strengths is desired [34].

To determine the effect of the $^{26}\text{Al}^m(p,\gamma)^{27}\text{Si}$ reaction rate on the overall production of ^{26}Al in ONe novae, resonances below 445 keV must be directly measured, and such an effort has been proposed [35]. This work provides motivation for undertaking such a measurement and gives information on where specific resonances at energies ≥ 445 keV are located. By providing the first extensive experimentally determined $^{26}\text{Al}^m + p$ resonance information, these new results have shown that previous $^{26}\text{Al}^m(p,\gamma)^{27}\text{Si}$ reaction rate calculations (based on the scaling of experimentally determined $^{26}\text{Al}^g(p,\gamma)^{27}\text{Si}$ reaction rates) are inadequate, and further experimental study of $^{26}\text{Al}^m + p$ resonances is needed.

ACKNOWLEDGMENTS

Jac Caggiano provided much insight with regards to the technical and physical aspects of this experiment. We are

indebted to the staff at WNSL and acknowledge the support of US Department of Energy under Grant No. DE-FG02-91ER-40609.

-
- [1] T. Lee and D. A. Papanastassiou, *Geophys. Res. Lett.* **1**, 225 (1974).
- [2] J. G. Bradley, J. C. Huneke, and G. J. Wasserburg, *J. Geophys. Res.* **83**, 244 (1978).
- [3] J. José, M. Hernanz, S. Amari, K. Lodders, and E. Zinner, *Astrophys. J.* **612**, 414 (2004).
- [4] L. R. Nittler and P. Hoppe, *Astrophys. J.* **631**, L89 (2005).
- [5] W. A. Mahoney, J. C. Ling, W. A. Wheaton, and A. S. Jacobson, *Astrophys. J.* **286**, 578 (1984).
- [6] V. Schönfelder and M. Varendorf, *AIP Conf. Proc.* **232**, 101 (1991).
- [7] J. E. Naya, S. D. Barthelmy, L. M. Bartlett, N. Gehrels, M. Leventhal, A. Parsons, B. J. Teegarden, and J. Tueller, *Nature* **384**, 44 (1996).
- [8] R. Diehl *et al.*, *Astron. Astrophys.* **298**, 445 (1995).
- [9] D. M. Smith, *Astrophys. J.* **589**, L55 (2003).
- [10] R. Diehl, *New Astron. Rev.* **50**, 534 (2006).
- [11] J. José, M. Hernanz, and A. Coc, *Astrophys. J.* **479**, L55 (1997).
- [12] C. Ruiz *et al.*, *Phys. Rev. Lett.* **96**, 252501 (2006).
- [13] S. A. Mozkowski, *Beta- and Gamma-Ray Spectroscopy*, edited by K. Siegbahn (Interscience, New York, 1955).
- [14] R. A. Ward and W. A. Fowler, *Astrophys. J.* **238**, 266 (1980).
- [15] R. C. Runkle, A. E. Champagne, and J. Engel, *Astrophys. J.* **556**, 970 (2001).
- [16] L. Buchmann, M. Hilgemeier, A. Krauss, A. Redder, C. Rolfs, H. P. Trautvetter, and T. R. Donoghue, *Nucl. Phys.* **A415**, 93 (1984).
- [17] P. Schmalbrock, T. R. Donoghue, M. Wiescher, V. Wijekumar, C. P. Browne, A. A. Rollefson, C. Rolfs, and A. Vliet, *Nucl. Phys.* **A457**, 182 (1986).
- [18] R. B. Vogelaar, L. W. Mitchell, R. W. Kavanagh, A. E. Champagne, P. V. Magnus, M. S. Smith, A. J. Howard, P. D. Parker, and H. A. O'Brien, *Phys. Rev. C* **53**, 1945 (1996).
- [19] R. Lewis, J. Caggiano, A. Parikh, C. Deibel, D. Visser, K. Fear, P. Parker, and W. R. Hix, *Nucl. Phys.* **A758**, 84c (2005).
- [20] C. Angulo *et al.*, *Nucl. Phys.* **A656**, 3 (1999).
- [21] C. M. Deibel, Ph.D. thesis, Yale University, 2008.
- [22] T. F. Wang, A. E. Champagne, J. D. Hadden, P. V. Magnus, M. S. Smith, A. J. Howard, and P. D. Parker, *Nucl. Phys.* **A499**, 546 (1989).
- [23] T. J. Ognibene, J. Powell, D. M. Moltz, M. W. Rowe, and J. Cerny, *Phys. Rev. C* **54**, 1098 (1996).
- [24] A. Parikh, Ph.D. thesis, Yale University, 2006.
- [25] National Nuclear Data Center, information extracted from the chart of nuclides database, <http://www.nndc.bnl.gov/chart/>.
- [26] A. J. Ferguson, *Angular Correlation Methods in Gamma-ray Spectroscopy* (Wiley, New York, 1965).
- [27] J. W. Noé, D. P. Balamuth, and R. W. Zurmühle, *Phys. Rev. C* **9**, 132 (1974).
- [28] L. Lyons, *Statistics for Nuclear and Particle Physicists* (Cambridge University Press, Cambridge, 1986).
- [29] C. Iliadis, L. Buchmann, P. M. Endt, H. Herndl, and M. Wiescher, *Phys. Rev. C* **53**, 475 (1996).
- [30] C. M. Deibel, J. A. Clark, R. Lewis, A. Parikh, P. D. Parker, and C. Wrede (in preparation).
- [31] D. W. Bardayan *et al.*, *Phys. Rev. C* **74**, 045804 (2006).
- [32] P. N. Peplowski *et al.*, *Phys. Rev. C* **79**, 032801(R) (2009).
- [33] C. Wrede, *Phys. Rev. C* **79**, 035803 (2009).
- [34] A. A. Chen *et al.*, TRIUMF proposal S922 (unpublished).
- [35] C. Ruiz *et al.*, TRIUMF proposal S989 (unpublished).